LETTERS

Architecture of ribonucleoprotein complexes in influenza A virus particles

Takeshi Noda[1,2,3], Hiroshi Sagara[4], Albert Yen[5], Ayato Takada[3,6]†, Hiroshi Kida[2], R. Holland Cheng[5,7] & Yoshihiro Kawaoka[1,3,6,8]

In viruses, as in eukaryotes, elaborate mechanisms have evolved to protect the genome and to ensure its timely replication and reliable transmission to progeny. Influenza A viruses are enveloped, spherical or filamentous structures, ranging from 80 to 120 nm in diameter[1]. Inside each envelope is a viral genome consisting of eight single-stranded negative-sense RNA segments of 890 to 2,341 nucleotides each[1]. These segments are associated with nucleoprotein and three polymerase subunits, designated PA, PB1 and PB2; the resultant ribonucleoprotein complexes (RNPs) resemble a twisted rod (10–15 nm in width and 30–120 nm in length) that is folded back and coiled on itself[2–4]. Late in viral infection, newly synthesized RNPs are transported from the nucleus to the plasma membrane, where they are incorporated into progeny virions capable of infecting other cells. Here we show, by transmission electron microscopy of serially sectioned virions, that the RNPs of influenza A virus are organized in a distinct pattern (seven segments of different lengths surrounding a central segment). The individual RNPs are suspended from the interior of the viral envelope at the distal end of the budding virion and are oriented perpendicular to the budding tip. This finding argues against random incorporation of RNPs into virions[5], supporting instead a model in which each segment contains specific incorporation signals that enable the RNPs to be recruited and packaged as a complete set[6–12]. A selective mechanism of RNP incorporation into virions and the unique organization of the eight RNP segments may be crucial to maintaining the integrity of the viral genome during repeated cycles of replication.

To elucidate the architecture of the virion interior, we longitudinally and transversely sectioned A/WSN/33 (H1N1) virions budding from Madin–Darby canine kidney (MDCK) cells at 10 h after infection. Although A/WSN/33 virions released into culture medium are spherical in shape[13], the budding virions in longitudinal sections were elongated and contained rod-like structures that were associated with host-derived lipid bilayer envelopes and oriented perpendicular to the budding tip of the virion (Fig. 1a and Supplementary Fig. 1). They were ~12 nm in width and up to 130 nm in length, consistent with the sizes of purified RNPs[2–4]. In transversely sectioned budding virions, electron-dense dots, representing the rod-like structures seen in longitudinal sections, were apparent inside each virion (Fig. 1b). Notably, many of the virions contained eight dots, arranged as seven in a circle surrounding one at the centre (Fig. 1c); not more than eight dots were observed in a virion. To determine the lengths of the rod-like structures, we compared serial transverse sections of whole budding virions (Fig. 1d and Supplementary Fig. 2). In all virions examined, the number of dots decreased progressively with increasing distance from the budding tip of the virion. Together, these results indicate that influenza A virions contain a highly organized set of eight rod-like structures of different lengths (Fig. 2).

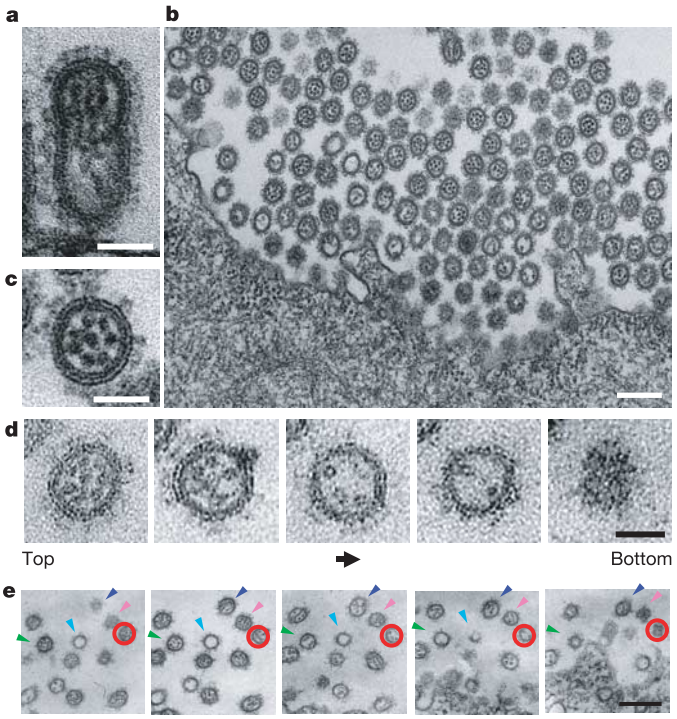

Figure 1 | Budding virions show a specific arrangement of eight rod-like structures of different lengths. **a**, Rod-like structures, 12 nm in width, are associated with the viral envelope at the distal end of the budding virion. **b**, **c**, Electron-dense dots ($N \leq 8$), representing transversely sectioned rods, were observed in each virion in a characteristic configuration (several peripheral dots surrounding a core dot). **d**, Serial sections of a virion cut from the distal end. As the distance from the end increased the number of dots decreased, suggesting that the eight rod-like structures differed in length. **e**, Lower magnification views of the serial ultrathin sections in **d**, demonstrating that the serial section shown in **d** represents the same virion (circled in red). Other virions are indicated by arrowheads. Scale bars, 50 nm (**a**, **c**, **d**); 200 nm (**b**, **e**).

[1]Internal Research Center for Infectious Diseases, Institute of Medical Science, University of Tokyo, Shirokanedai, Minato-ku, Tokyo 108-8639, Japan. [2]Laboratory of Microbiology, Department of Disease Control, Graduate School of Veterinary Medicine, Hokkaido University, Kita-ku, Sapporo 060-0818, Japan. [3]Core Research for Evolutional Science and Technology, Japan Science and Technology Agency, Kawaguchi, Saitama 332-0012, Japan. [4]Fine Morphology Laboratory, Department of Basic Medical Science, and Division of Virology, Institute of Medical Science, University of Tokyo, Shirokanedai, Minato-ku, Tokyo 108-8639, Japan. [5]Department of Biosciences, Karolinska Institute, 141 57 Huddinge, Sweden. [6]Department of Microbiology and Immunology, Institute of Medical Science, University of Tokyo, Shirokanedai, Minato-ku, Tokyo 108-8639, Japan. [7]Molecular and Cellular Biology, University of California, Davis, California 95616, USA. [8]Department of Pathological Science, School of Veterinary Medicine, University of Wisconsin-Madison, Madison, Wisconsin 53706, USA. †Present address: Research Center for Zoonosis Control, Hokkaido University, Kita-ku, Sapporo 060-0818, Japan.

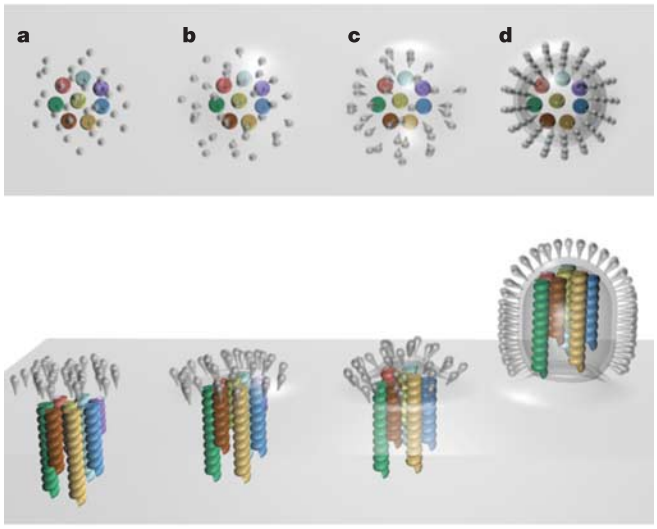

Figure 2 | Rod-like structures in a developing virion. a–c, Rod-like structures align vertically with the plasma membrane. **d**, The fully developed budding virion contains a set of eight rod-like structures. Virions in the upper row are viewed from the top; those in the lower row are shown in side profile.

To determine whether or not the arrangement of the virion interior in spherical A/WSN/33 virus is unique to that strain, we examined MDCK cells infected with other strains of spherical influenza A viruses isolated from humans (A/Aichi/2/68 (H3N2) and A/Puerto Rico/8/34 (H1N1)), ducks (A/duck/Hong Kong/836/80 (H3N1) and A/mallard/New York/6750/78 (H2N2)), and swine (A/swine/Chiba/1/91 (H1N2); see Supplementary Fig. 3). In all strains tested, the virions showed the same organization of rod-like structures, in which a central dot was surrounded by seven dots, duplicating the pattern seen in A/WSN/33 virions.

Because some influenza A viruses, especially newly isolated strains, are filamentous[1], we next examined the architecture of the filamentous A/Udorn/307/72 (H3N2) virus. Although most of the transverse sections of filamentous virions lacked electron-dense material (Supplementary Fig. 4a), some showed the typical configuration of seven dots with a single core dot (Supplementary Fig. 4b). In longitudinally sectioned filamentous virions, the rod-like structures were confined to the distal end of each filamentous particle (Supplementary Fig. 4c); the remainder of the virion was empty, consistent with the apparent lack of internal structures in transverse sections of filamentous virions. Thus, both spherical and filamentous influenza virions budding from cells possess an organized set of eight rod-like structures that are associated with the envelope at the budding end of the virion.

Our serendipitous observation that some influenza A virions are partially disrupted when freeze-dried enabled us to study the nature of the rod-like structures inside virions. The widths of the structures released by freeze-dried, negatively stained A/Puerto Rico/8/34 virions were ~12 nm on average (Fig. 3a), similar to the widths of structures inside sectioned virions (Fig. 1). These released structures were morphologically indistinguishable from the RNPs purified from virions in previous studies[2–4] and reacted with anti-nucleoprotein monoclonal antibodies conjugated to colloidal gold (Fig. 3b). To determine further the nature of the rod-like structures observed in virions, we performed ultrathin-section immunoelectron microscopy using mouse monoclonal antibody against nucleoprotein. The electron-dense dots in transversely sectioned virions reacted with anti-nucleoprotein monoclonal antibodies conjugated to gold particles (Fig. 3c), indicating that they were indeed viral RNPs.

To analyse the interior architecture of virions in greater detail, we used electron tomography, which constructs a three-dimensional density map of molecules, the 'tomogram', at a near-molecular resolution[14]. Taking computational thin slices from the map, Fig. 4 shows the results of electron tomography applied to virions budding from MDCK cells. Within a virion, outlined in Fig. 4 by a bilayered membrane with protruding viral glycoproteins, were eight RNPs with a distorted round or square shape. Although some of the RNPs were clearly isolated from each other, there were instances in which peripheral RNPs, as well as central and peripheral RNPs, appeared to be in close contact (Fig. 4, arrows). Whether such contact represents nonspecific association of the RNPs inside the virion or specific interactions with functional significance remains to be determined.

Our findings address a long-standing controversy in influenza virus research: are viral RNA segments incorporated randomly[5] or selectively[6,7] into virions? Together with studies showing that all viral RNPs possess segment-specific packaging signals (refs 8–12; and Y. Muramoto and Y.K., and M. Ozawa and Y.K., unpublished data), our morphological findings clearly favour a model of selective incorporation. Still unclear is how the eight RNPs are organized into a characteristic arrangement within virions. One possibility is that coding regions of the viral RNAs possess signal sequences that promote recruitment of the segments during virion assembly[8], which may then control intersegmental association. Our study contributes

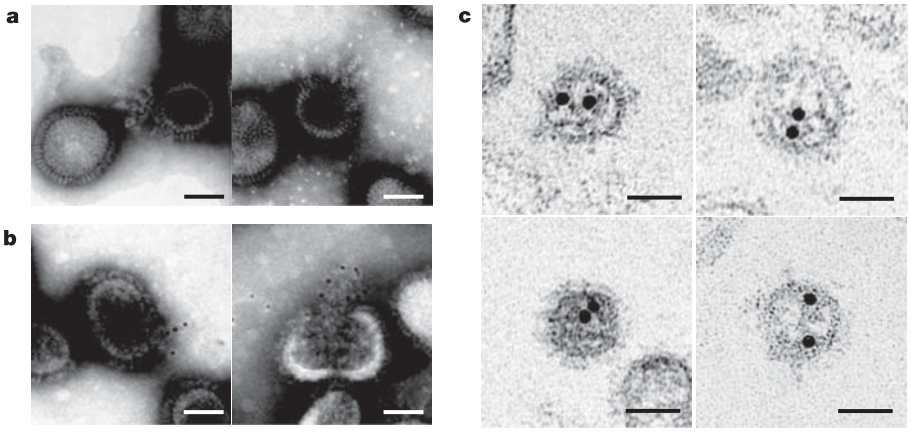

Figure 3 | Identification of rod-like structures in virions as viral RNPs. a, Virions ruptured by freeze-drying release twisted rods, 12 nm in width, which are indistinguishable from described purified RNPs[2–4]. **b**, Twisted rods specifically immunolabelled with anti-nucleoprotein monoclonal antibodies conjugated to 5-nm gold particles. **c**, Immunogold labelling of electron-dense dots within transversely sectioned virions with anti-NP monoclonal antibodies conjugated to 10-nm gold particles. Scale bars, 50 nm.

Figure 4 | Electron tomography of RNP complexes in a budding virion. The virion was reconstructed in three dimensions by electron tomography, and three tomograms of its upper portion (at 2.15-nm intervals) containing eight RNPs are shown. Note the close proximities (possible associations) of the RNPs (arrows). Scale bar, 50 nm.

fundamental knowledge to attempts aimed at elucidating the mechanisms of genome incorporation into virions. Defining the interior architecture of influenza virions may speed up the development of both antiviral compounds and more efficient methods of gene delivery and expression.

METHODS

Cells and viruses. A stock of A/WSN/33 (H1N1) was prepared by growing the virus in MDCK cells. Stocks of A/Aichi/2/68 (H3N2), A/Puerto Rico/8/34 (H1N1), A/duck/Hong Kong/836/80 (H3N1), A/mallard/New York/6750/78 (H2N2), A/swine/Chiba/1/91 (H1N2) and A/Udorn/307/72 (H3N2) were prepared in embryonated chicken eggs aged 10–11 d.

Ultrathin section electron microscopy. Electron microscopy was done as described[15]. In brief, MDCK cells were infected with virus at a multiplicity of infection of more than 10 and were then prefixed with 2.5% glutaraldehyde in 0.1 M cacodylate buffer (pH 7.4) on ice for 1 h. After being washed with the same buffer, the cells were post-fixed with 2% osmium tetraoxide on ice for 1 h, stained with uranyl aqueous solution *en bloc*, dehydrated with a series of ethanol gradients followed by propylene oxide treatment, and embedded in Epon 812 Resin mixture. Ultrathin sections (~60-nm thick) were stained with 2% uranyl acetate in 70% ethanol for 3 min at room temperature and in Raynold's lead for 3 min at room temperature, and then examined with a JEM-1200EX electron microscope (Jeol) operated at 80 kV. For ultrathin section-immunoelectron microscopy, the sections were prepared on nickel grids as described above and incubated with saturated sodium periodate solution[16,17], followed by 0.2 M glycine in PBS buffer. After being washed with PBS, the sections were incubated with 1% bovine serum albumin (BSA) in PBS, and then with anti-influenza A virus nucleoprotein mouse monoclonal antibodies. They were then washed with PBS and incubated with a goat anti-mouse immunoglobulin conjugated to 10-nm gold particles (1:100 dilution, BBInternational).

Preparation of serial ultrathin sections. Samples for serial ultrathin sections were prepared as described above. Sections (~20-nm thick) were continuously cut with an Ultracut S ultramicrotome (Leica). The resultant series of ultrathin sections were placed on a single-slot copper grid and examined with an H-7500 electron microscope (Hitachi) operated at 60 kV.

Negative staining of freeze-dried samples. Purified virions were adsorbed to Formvar-carbon-coated copper grids and negatively stained with 2% phosphotungstic acid solution (PTA). Grids were immediately placed in liquid nitrogen and transferred to a JEE-4X vacuum evaporator (Jeol) for freeze-drying. Immunoelectron microscopy was done with freeze-dried samples on nickel grids treated as described above, except that the 2% PTA staining step was omitted. The grids were then treated with 1% BSA in PBS and mouse monoclonal antibodies against influenza A virus nucleoprotein, washed with PBS, and incubated with a goat anti-mouse immunoglobulin conjugated to 5-nm gold particles (1:50 dilution, BBInternational). After being washed, the samples were fixed with 2% glutaraldehyde and negatively stained with 2% PTA.

Tomographic reconstruction. Sections (~50-nm thick) were prepared as described above and affixed to 10-nm colloidal gold particles on the upper surface, which served as fiducial markers for subsequent image alignment. They were then placed in a CompStage specimen holder (FEI) and imaged in a Tecnai G2 Shera (FEI) operating at 200 kV. Images were taken at a magnification of 58,000 every 2° (from −65° to +70°) and recorded by a Gatan CCD camera (1,024 × 1,024 pixels with 0.43 nm per pixel) with an accumulative electron dose of 400 e^{-} A^{-2}. The alignment of the projections was calculated by using IMOD software[18] and the 10-nm gold beads, and the three-dimensional reconstruction was based on an *R*-weighted back projection. Galleries of slice tomograms were displayed with Amira software (Template Graphics) at intervals of 2.15-nm voxels.

Received 26 August; accepted 26 October 2005.

1. Lamb, R. A. & Krug, R. M. in *Fields Virology* (eds Knipe, D. M. & Howley, P. M.) 1487–1532 (Lippincott, Williams & Wilkins, Philadelphia, 2001).
2. Compans, R. W., Content, J. & Duesberg, P. H. Structure of ribonucleoprotein of influenza virus. *J. Virol.* **10,** 795–800 (1972).
3. Heggeness, M. H. *et al.* Studies on the helical nucleocapsid of influenza virus. *Virology* **118,** 466–470 (1982).
4. Oxford, J. S. & Hockley, D. J. *Orthomyxoviridae. Animal Virus Structure* 213–232 (Elsevier, Amsterdam, 1987).
5. Enami, M., Sharma, G., Benham, C. & Palese, P. An influenza virus containing nine different RNA segments. *Virology* **185,** 291–298 (1991).
6. Duhaut, S. D. & McCauley, J. W. Defective RNAs inhibit the assembly of influenza virus genome segments in a segment-specific manner. *Virology* **216,** 326–337 (1996).
7. Odagiri, T. & Tashiro, M. Segment-specific noncoding sequences of the influenza virus genome RNA are involved in the specific competition between defective interfering RNA and its progenitor RNA segment at the virion assembly step. *J. Virol.* **71,** 2138–2145 (1997).
8. Fujii, Y. *et al.* Selective incorporation of influenza virus RNA segment into virions. *Proc. Natl Acad. Sci. USA* **100,** 2002–2007 (2003).
9. Watanabe, T. *et al.* Exploitation of nucleic acid packaging signals to generate a novel influenza virus-based vector stably expressing two foreign genes. *J. Virol.* **77,** 10575–10583 (2003).
10. Fujii, K. *et al.* Importance of both the coding and the segment-specific noncoding regions of the influenza A virus NS segment for its efficient incorporation into virions. *J. Virol.* **79,** 3766–3774 (2005).
11. Liang, Y., Hong, Y. & Parslow, T. G. *cis*-Acting packaging signals in the influenza virus PB1, PB2, and PA genomic RNA segments. *J. Virol.* **79,** 10348–10355 (2005).
12. Dos Santos Afonso, E. *et al.* The generation of recombinant influenza A viruses expressing a PB2 fusion protein requires the conservation of a packaging signal overlapping the coding and noncoding regions at the 5′ end of the PB2 segment. *Virology* **341,** 34–46 (2005).
13. Schulze, I. T. The structure of influenza virus. *Virology* **42,** 890–904 (1970).
14. Medalia, O. *et al.* Macromolecular architecture in eukaryotic cells visualized by cryoelectron tomography. *Science* **298,** 1209–1213 (2002).
15. Noda, T. *et al.* Ebola virus VP40 drives the formation of virus-like filamentous particles along with GP. *J. Virol.* **76,** 4855–4865 (2002).
16. Bendayan, M. & Zollinger, M. Ultrastructural localization of antigenic sites on osmium-fixed tissues applying the protein A–gold technique. *J. Histochem. Cytochem.* **31,** 101–109 (1983).
17. Bendayan, M. & Maestracci, N. D. Pituitary adenomas: patterns of hPRL and hGH secretion as revealed by high resolution immunocytochemistry. *Biol. Cell* **52,** 129–138 (1984).
18. Kremer, J. R., Mastronarde, D. N. & McIntosh, J. R. Computer visualization of three-dimensional image data using IMOD. *J. Struct. Biol.* **116,** 71–76 (1996).

Supplementary Information is linked to the online version of the paper at www.nature.com/nature.

Acknowledgements We thank J. Gilbert for editing the manuscript; M. Imai, Y. Muramoto and K. Fujii for discussion; Y. Hirata, K. Aoyama and K. Inoke for technical assistance with electron microscopic tomography; and Y. Kawaoka for illustrations. This work was supported by CREST (Japan Science and Technology Agency), by Grants-in-Aid by the Ministry of Education, Culture, Sports, Science and Technology, by the Ministry of Health, Labor and Welfare, Japan, and by a National Institute of Allergy and Infectious Disease Public Health Service research grant (to Y.K.); and by Swedish Research Council grants and the STINT Foundation (to R.H.C.). T.N. was the recipient of a fellowship from the incorporated foundation SYOUSHISYA and a research fellowship from the Japan Society for the Promotion of Science for Young Scientists.

Author Information Reprints and permissions information is available at npg.nature.com/reprintsandpermissions. The authors declare no competing financial interests. Correspondence and requests for materials should be addressed to Y.K. (Kawaoka@ims.u-tokyo.ac.jp).